Pressurized two-electrode spark gap with saturable inductance

Part 1: Experiments with various ferrite materials

E. v. Mark, H. Wedler

IPP 4/54 June, 1968

INSTITUT FÜR PLASMAPHYSIK

GARCHING BEI MÜNCHEN

INSTITUT FÜR PLASMAPHYSIK

GARCHING BEI MÜNCHEN

Pressurized two-electrode spark gap with saturable inductance

Part 1: Experiments with various ferrite materials

E. v. Mark, H. Wedler

IPP 4/54 June, 1968

Die nachstehende Arbeit wurde im Rahmen des Vertrages zwischen dem Institut für Plasmaphysik GmbH und der Europäischen Atomgemeinschaft über die Zusammenarbeit auf dem Gebiete der Plasmaphysik durchgeführt.

Abstract

Initial results in developing a compact pressurized two-electrode spark gap with saturable inductance for heavy duty are given.

The first part of the paper describes experiments with various ferrite cores and ferrite materials. The maximum attainable voltage is defined as a function of the pulse steepness, the ferrite material, and the saturated inductance L_{Fe_o}

In the second part the pulse breakdown voltage is investigated in pressurized air. The results show good agreement with calculations. Experiments with a 40 kJ standard unit are conducted to clarify problems such as arc migration and minimum electrode distance.

The results of the investigations are used to design a pressurized spark gap with the following data:

Static breakdown voltage:	V_s	=	60 kV
Total inductance:	L	=	30 nHy
Operating range at constant pressure:	35	-	60 kV
Trigger pulse steepness:	5	-	10 kV/nsec

The characteristic jitter is low, because the jitter only depends on the trigger pulse.

Contents

Figures of the appendix

1. General

The ferrite-decoupled crowbar spark gaps (L 1, L 2, L 3) used in the Isar 1, Isar 2, Isar 3, Isar 4, and turbulence heating experiments at Garching have not given any trouble. This prompted us to attempt similar solutions for starting switches.

The most important advantages of a two-electrode spark gap are as follows:

a) Simple design (2 electrodes)

b) Low characteristic jitter, because jitter is only dependent on trigger pulse steepness

c) Lower ohmic losses (2 arc spots)

d) Lower inductance of the arc channel

e) Less probability of premature breakdown (only 1 separating gap)

f) No dynamic stabilization necessary

g) Improved arc migration

The gap ($\eta > 90$ %) has to be triggered in one stage, but the fairly high trigger voltage required does not present any special problems at the present charging voltages of the energy stores ($V_{co} \sim 40$ kV). The additional inductance due to the necessary decoupling is of the order of 10 ...30 nHy, and in many cases this can be kept even smaller if regions of discrete inductance L_d, such as the cable terminals, afford additional decoupling. For an arc length of 3 - 5 mm ($L \sim 5$ nHy) the total inductance of such a spark gap is 15 - 35 nHy, and so, with regard to the inductive component, it can compete with conventional trigatron or cascade spark gaps (L 6, L 7, L 8, L 9).

./.

The overvolted two electrode spark gap proposed by various authors (L 4, L 5) usually cannot be used in the low-impedance magnetic field devices for plasma research (fast magnetic compression) without considerable technical outlay. The steep and high trigger pulses required limit this type at present to a very few applications.

Prior to the investigations proper, the problems entailed by a two-electrode spark gap were systematically set out (fig. 1-A, p. 20). The individual parameters are ordered to yield the diagram with different developing stages shown in fig. 2-A, p. 21, the principal features being as follows:

1) Theoretical considerations and calculations
2) Experiments with various ferrite materials
3) Investigation of pulse breakdown in air
4) Migration, erosion and insulation problems
5) Experiments with various prototypes
6) Development of a suitable trigger system

At first attention will be concentrated on points 2 and 3. The investigation of the pulse breakdown in air with voltage waves rising linearly (voltage gradient $\frac{dV}{dt}$ = 1 ... 10 kV/nsec) in various gases is important for the development of spark gaps. The purpose of the present investigations is to find a gaseous dielectric with selective behaviour (fig. 1).

Migration and erosion problems are only included in the investigations because the proposed spark gap is intended for high duty comparable with that occuring in the case of dielectric switches. An important question in this connection is the minimum distance which should be observed in pressurized spark gaps. This problem arises because the pulse breakdown factor decreases at constant breakdown voltage with increasing pressure (fig. 19-A). The spark gap should therefore

./.

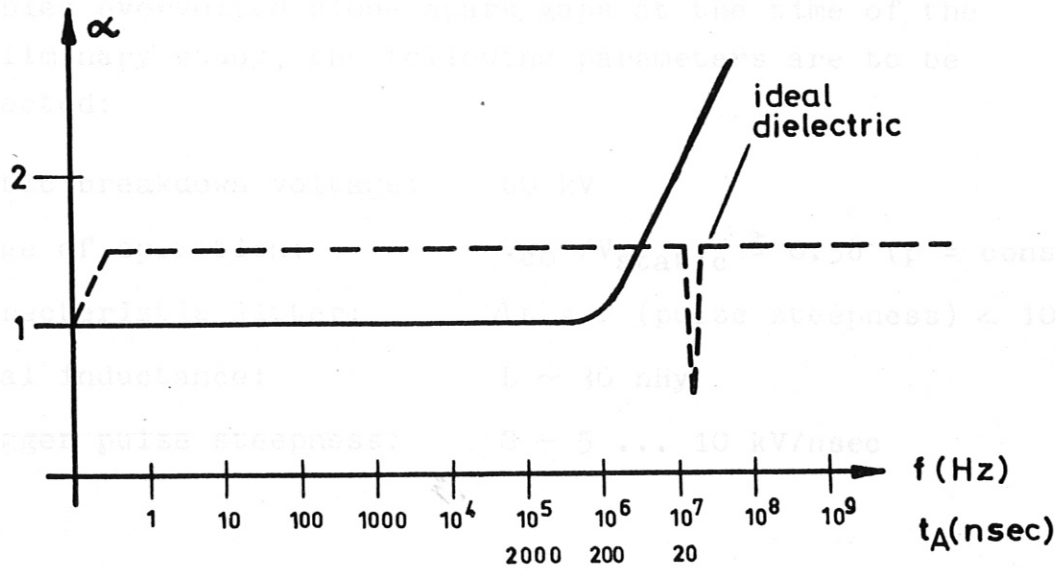

fig. 1: Band-pass behaviour of an ideal dielectric and low-pass behaviour of air under pulsed stress

be operated with the smallest possible separation and correspondingly high pressure. This is complicated, however, by the fact that with small separations the static breakdown voltage is appreciably changed as a result of spike formation and erosion.

Of decisive importance for two-electrode spark gaps is the solution of the trigger problem. The additional inductance required depends strongly on the pulse steepness ($S = \frac{dV}{dt}$) and the impedance of the trigger cable. The proposed trigger system is discussed in a separate paper. The importance of the trigger problem emerges from the fact that, with appropriately steep voltage pulses in conjunction with as small a characteristic impedance of the cable lead as possible, the overvolted diode spark gap constitutes the ideal switch.

./.

2. Preliminary theoretical investigations

On the basis of the data available on additionally decoupled overvolted diode spark gaps at the time of the preliminary study, the following parameters are to be expected:

Static breakdown voltage:	60 kV
Range of operation:	$V_{co}/V_{static} \geq 0.58$ (p = const)
Characteristic jitter:	Δt = f (pulse steepness) $\leq$ 10 nsec
Total inductance:	L ~ 30 nHy
Trigger pulse steepness:	S ~ 5 ... 10 kV/nsec

2.1 Principle of an overvolted two-electrode spark gap decoupled by saturation inductance

The devices used in plasma physics for fast magnetic compression have to have as low inductance as possible. The inductances and ohmic resistances have to be smaller than the corresponding values of the load: $L_c, L \ll L_v$

$R_c, R \ll R_v$

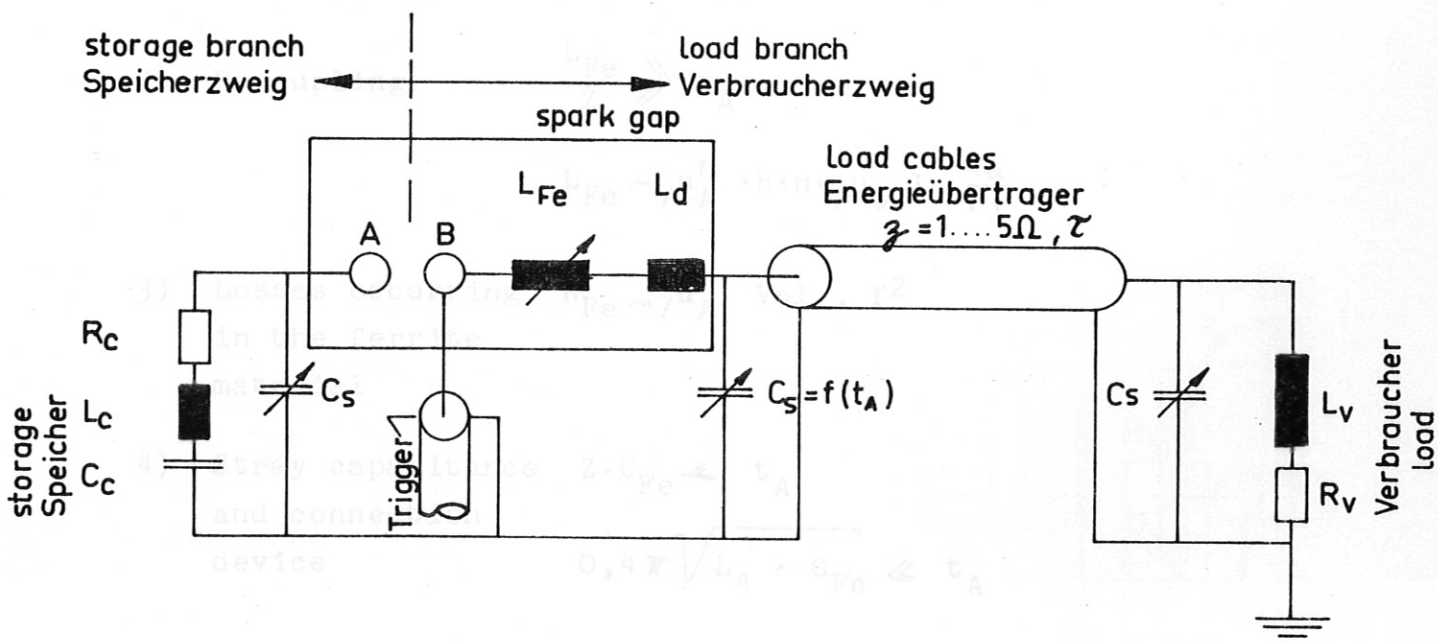

fig. 2: Equivalent circuit diagram of a capacitor bank for fast magnetic compression (rise times $t_A < \tau$)

./.

Figure 2 shows an equivalent circuit diagram of a bank. In fig. 3-A on p. 22, the equivalent circuits applicable for various pulse steepnesses are set out. The stray capacitance C_s, which serves as variable, more or less includes the capacitance of the load cables, depending on the pulse steepness.

The principle of the spark gap shown is simple. By means of the additional saturable inductance L_{Fe} (the arrangements used here are coaxial and have ferrite cores), marked in the diagram, it is possible to raise the decoupled electrode B until the gap A-B breaks down. The discrete inductance L_d (e.g. cable terminal) shown in fig. 2 is normally not sufficient for decoupling. The inductance can, however, contribute to a reduction of L_{Fe}. In the experiments described here, it is assumed that $L_d = 0$. (A more detailed account is given in L 2, L 3).

The maximum attainable voltage $\hat{V}_{Fe}$ at the decoupling depends on the:

1) Induction $$\int_{t=o}^{t=t_{sat}} B \, dB \sim \int_{t=o}^{t=t_{sat}} v \, dt = \frac{1}{2}\hat{V}_{Fe} \cdot t_A = \frac{1}{2}\frac{\hat{V}^2_{Fe}}{S}$$

2) Decoupling $$\frac{L_{Fe}}{Z} \gg t_A$$

$$L_{Fe} \sim \mu'_A \cdot h \cdot n \cdot \mu_o \cdot \ln \frac{r_a}{r_i}$$

3) Losses occurring in the ferrite material $R_{Fe} \sim \mu''_A$, Vol., f^2

4) Stray capacitance and connection device $$Z \cdot C_{Fe} \ll t_A$$

$$0{,}4\pi\sqrt{L_A \cdot C_{Fe}} \ll t_A$$

./.

2.2 Possible modifications of a two-electrode spark gap

Version 1: Overvolted two-electrode spark gap (L 4)
a) not additionally irradiated
b) irradiated

Version 2: Steep overvolted two-electrode spark gap (L 5)

Version 3: Overvolted two-electrode spark gap with saturable inductance
a) not irradiated
b) irradiated (α, ß, γ, photons)
1. pulsed
2. stationary L_{Fe_o}

Version 4: Type 3 + premagnetization $\Longrightarrow L^{x}_{Fe_o} \sim 0{,}4\ L_{Fe_o}$

Version 5: Type 3 + pulse sharpening spark gap

Version 6: Type 3 + pulse sharpening gap and premagnetization (L 2, L 3)

Version 7: Type 3 + pulse sharpening gap + premagnetization + matching

We are developing the simplest version, namely (Type 3 b)1.). The interesting Type 4 is identical with Type 3. It merely calls for some elaboration of the trigger system in order to obtain the required pulse shape for premagnetization.

3. Experiments on saturable inductances

The experimental setup is shown in fig. 3.

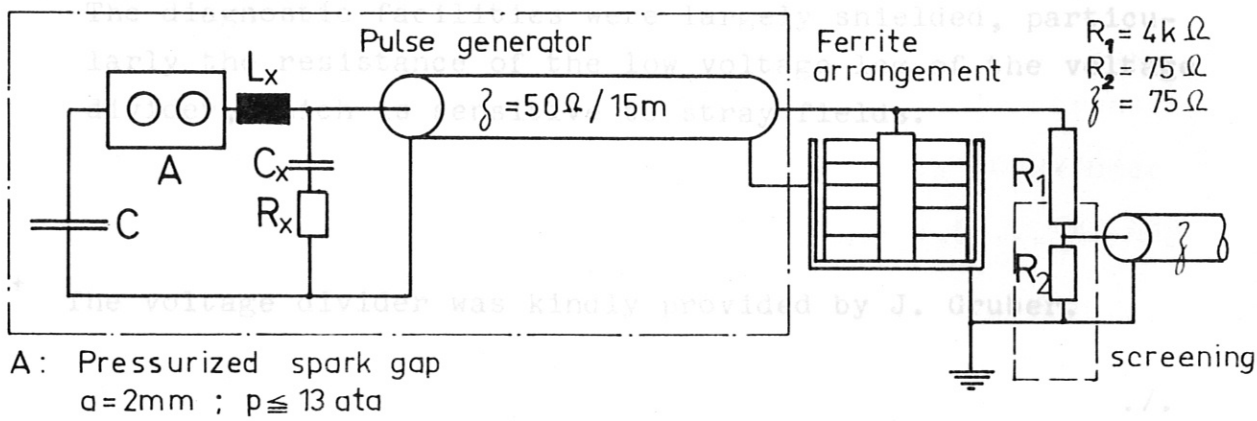

A: Pressurized spark gap
a=2mm ; p≦ 13 ata

fig. 3: Experimental setup for measurements on various ferrite cores.

./.

The experiment comprises two components:

a) Pulse generator with the following data:

peak voltage: $\hat{V}$ = 100 kV;

rise time t_A adjustable from 10 ... 100 nsec by varying the matching elements L_x, R_x, C_x;

pulse steepness: $S = \frac{dV}{dt}$ = 1 ... 10 kV/nsec;

deviation from linearity (10 % - 90 %) < 5 %

spark gap A: self-triggering pressurized spark gap;

for particularly fast pulses a generator with ceramic capacitors that is operated with a steepness of 20 kV/nsec and $\hat{V}$ = 100 kV was used.

b) Measuring circuit:

oscilloscope: Tektronix 507 with input direct on plates

rise time: t_A = 2.7 nsec $\hat{=}$ f_g = 70 Mc

calibration of time base: < 5 %;

morganite voltage divider +:

rise time: < 1 nsec;

deviation of transmission factor: < 7 %

rise time of the entire measuring system (507, delay line, voltage divider): t_A = 3 nsec.

The diagnostic facilities were largely shielded, particularly the resistance of the low voltage leg of the voltage divider, which is sensitive to stray fields.

+ The voltage divider was kindly provided by J. Gruber.

./.

3.1 Experimental results

3.1.1 In a series of experiments on various ferrite arrangements whose inductance in the saturated state was L_{Fe_o} = const = 20 nHy, the maximum attainable voltage $\hat{V}_{Fe}$ for constant voltage steepness S = 7 kV/nsec was determined. The results are listed in table (fig. 4-A, p. 23):

L_{Fe_o} = 20 nHy; n = variable
S = 7 kV/nsec; Dim: variable
Z = 50 Ω ;

3.1.2 The influence of the pulse steepness S was investigated in the five best types of core in the series 3.1.1 (fig. 5-A):

L_{Fe_o} = 20 nHy; n = variable
S = 1 ...20 kV/nsec; Dim: variable
Z = 50 Ω

3.1.3 Another five cores of varying quality but with the same dimensions (72 x 30 x 5 mm) were used for studying the influence of the pulse steepness and the ferrite material (fig. 6-A):

Dim: 72 x 30 x 5 mm S = 1 ... 10 kV/nsec
n : 10 L_{Fe_o} = 15 nHy
Z = 50 Ω

3.1.4 The influence of the number of ferrite cores on the maximum attainable voltage $\hat{V}_{Fe}$ can be seen in fig. 7-A. This series of measurements was made with various types of cores:

Dim: 72 x 30 x 5 mm S = 1 ... 10 kV/nsec
n : 5 ... 28 L_{Fe_o} = 7,5 ... 42 nHy
Z = 50 Ω

./.

3.2 Evaluation of results and tentative interpretation

The equivalent circuit diagram of the ferrite arrangement is shown in fig. 4. The simplification made here is possible by estimating the individual parameters.

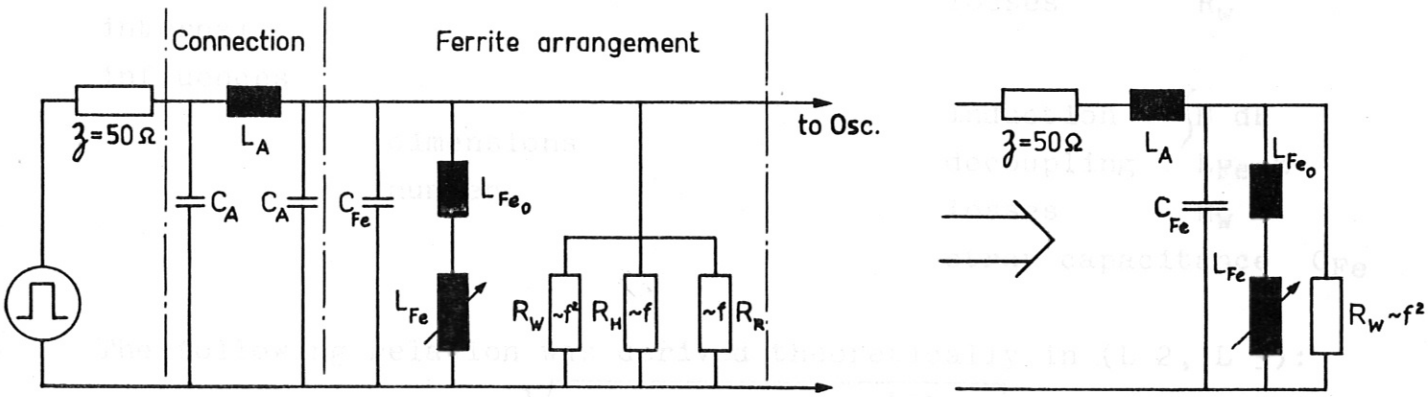

fig. 4: Equivalent circuit of a ferrite arrangement for fast processes ($t_A < 100$ nsec)

Simplified representation

The stray capacitance of the ferrite arrangement with 20 cores (72 x 30 x 5 mm) is C_{Fe} = 35 pF. The connection inductance L_A is about 40 nHy. The hysteresis losses (R_H) and remanence losses (R_R) can easily be neglected in non-recurring processes. The possible representation of the ferrite arrangement as a delay network is no longer justified for the very high ratio $L_{Fe}/C_{Fe} \sim 10^6$ that is normally obtained. In the case of very slow pulses, which are uninteresting for our purposes, equivalent circuits similar to those in fig. 3-A are obtained.

From a purely schematical point of view, it is possible to fix the following parameters which largely influence the peak voltage $\hat{V}_{Fe}$:

./.

external influences	steepness of voltage pulse S		
	impedance of cable Z		
	connection inductance L_A		
internal influences	ferrite material	induction	$\int B\ dB$
		decoupling	L_{Fe}/Z
		losses	R_W
	dimensions number	induction	$\int B\ dB$
		decoupling	L_{Fe}/Z
		losses	R_W
		stray capacitance	C_{Fe}

The following relation was derived theoretically in (L 2, L 3):

$$\hat{V}_{Fe} = \sqrt{S \cdot h \cdot n(r_a - r_i) \cdot \int_{t=0}^{t=t_{sat}} B\ dB}$$

This derivation was made on the assumption:

$$u_A = \text{const.} \quad (t < t_{sat},\ H < H_{sat})$$

$$\frac{L_{Fe}}{Z} \gg t_A = \frac{\hat{V}_{Fe}}{S}$$

$$i_{sat} = 2\pi \cdot r_a \cdot H_{sat} \ll \frac{\hat{V}_{Fe}}{Z}$$

$$R_W \gg Z$$

$$0{,}4 \cdot \pi \cdot \sqrt{L_A \cdot C_{Fe}} \ll t_A$$

$$Z \cdot C_{Fe} \ll t_A$$

3.2.1 Influence of pulse steepness

The measuring series (figs. 5-A, 6-A, and 7-A) confirm the relation $\hat{V}_{Fe} \sim k\sqrt{S}$. Above a certain steepness $S \mathrel{\hat{=}} f_g \mathrel{\hat{=}} t_A$ this proportionality is no longer obtained. For $S > S$ it holds that $k \sim \frac{1}{S}$. The relation $\hat{V}_{Fe} = f(S)$ is shown in fig. 5.

./.

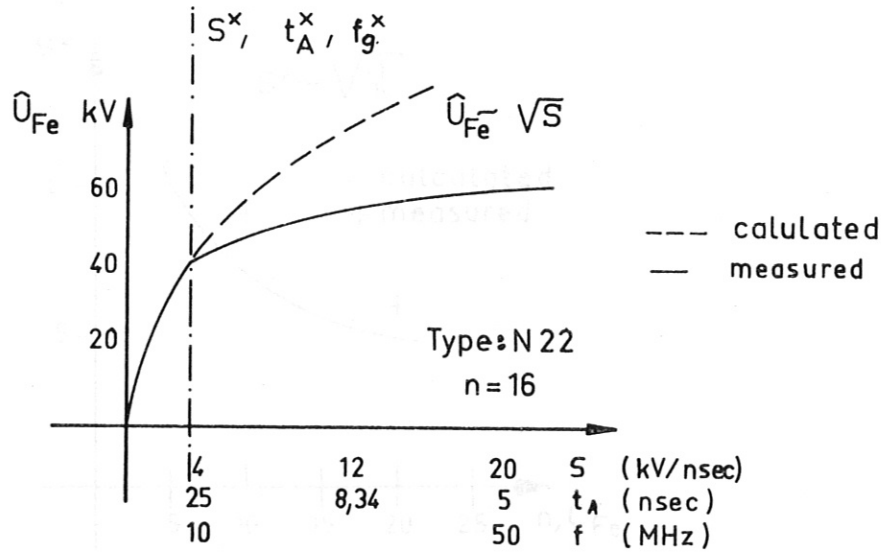

fig. 5: Influence of the pulse steepness on the maximum attainable voltage $\hat{V}_{Fe}$.

Possible explanations are the following:

1. Growth of eddy current losses $R_W \sim f^2$, n, Vol.
2. Decrease of the pulse steepness by the connection inductance L_A and the stray capacitance C_{Fe}.
3. The real part $'u_A'$ of the complex permeability decreases when a certain frequency is attained, thus reducing the decoupling.
4. The induction $\int B\,dB$, which governs the peak voltage $\hat{V}_{Fe}$, depends on the frequency and decreases above a certain frequency.

It is reasonable to suppose that all four factors may contribute to causing this characteristic dependence.

An estimate of the influence of L_A and C_{Fe} yield a resonance corresponding to 12,5 Mc $\hat{=}$ t_A = 16,7 nsec $\Rightarrow$ S^* = 5 kV/nsec. Fig. 5 shows good agreement with this estimate (n= 16; N 22). The relation $S^* = 1/\sqrt{n}$ should generally be valid since $C_{Fe} \sim n$. Figure 6 shows the dependence $S^* = f(n)$. The experimental values taken from fig. 7-A deviate only slightly from the calculated curves.

./.

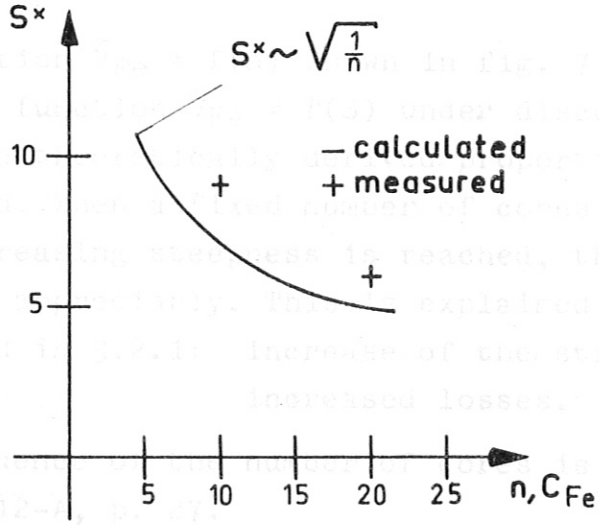

fig. 6: Influence of the stray capacitance $C_{Fe}(\sim n)$ on the limiting steepness

The known cut-off frequencies for various types of ferrite:

K 1 :	f_g = 40 Mc	N 27 :	f_g = 1 Mc
M 33 :	f_g = 3 Mc	T 35 :	f_g = 0,2 Mc
N 22 :	f_g = 2 Mc		

prove that the limiting steepness S^* can be influenced as well by the eddy current losses, which also become larger as the number of cores is increased.

No qualitative statement can be made about the influence of the induction $\int B\, dB$ on the function $\hat{V}_{Fe} = f(S)$ since only the static B-H characteristic curves are known.

In the case of more permeable cores with limiting frequencies $f_g < 2$ Mc, the dependence L_{Fe}/Z may lead to the decoupling being insufficient; if the last two factors were significant, the limiting steepness would, of course, grow as the number of cores increases ($S \sim \sqrt{n}$). In the regions investigated here this is not the case.

./.

3.2.2 Influence of number of cores

The relation $\hat{V}_{Fe} = f(n)$ shown in fig. 7-A is almost identical with the function $\hat{V}_{Fe} = f(S)$ under discussion. In a defined range the theoretically derived proportionality $\hat{V}_{Fe} \sim \sqrt{n}$ is satisfied. When a fixed number of cores that becomes smaller with increasing steepness is reached, the proportionality declines appreciably. This is explained by the phenomena mentioned in 3.2.1: increase of the stray capacitance
increased losses.

The influence of the number of cores is specially illustrated in fig. 12-A, p. 27.

3.2.3 Influence of core dimensions

The relation $\hat{V}_{Fe} \sim \sqrt{h \cdot n(r_a - r_i)}$ derived in L 3 was discussed with regard to the term h·n. The extent to which the influence $\hat{V}_{Fe} \sim \sqrt{r_a - r_i}$ is present could not be checked by the experiment. Only two types of core of various dimensions and made of the same material were available (fig. 5-A). The relation $\hat{V}_{Fe1}/\hat{V}_{Fe2}$ resulting from this series depends on the steepness of the pulse.

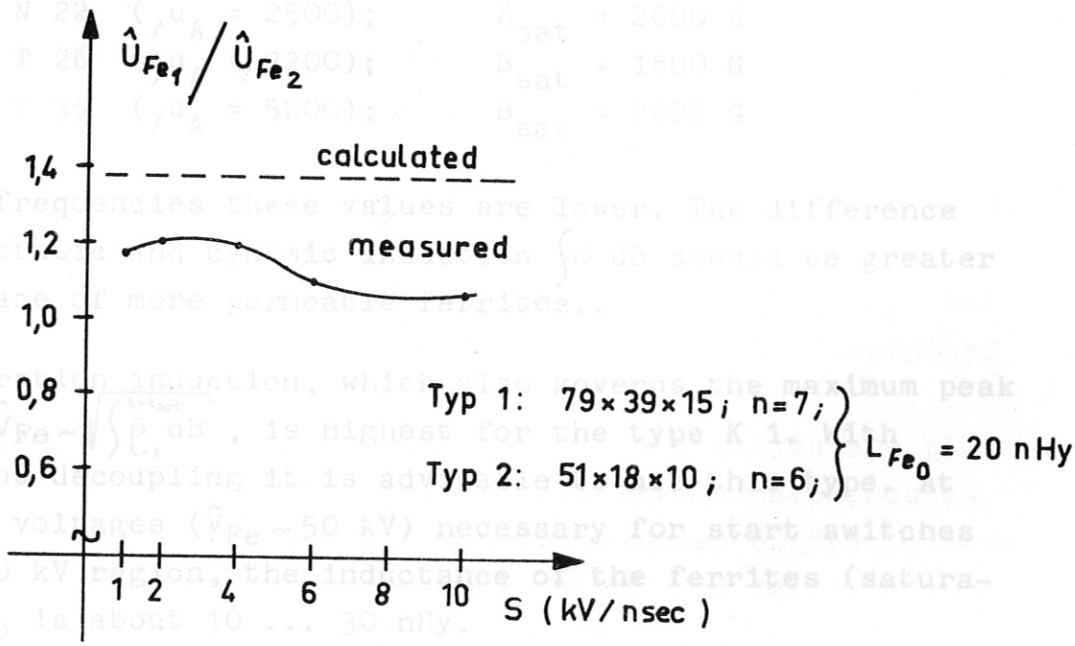

fig. 7: Influence of core dimensions on the maximum attainable voltage $\hat{V}_{Fe}$

The decrease $\hat{V}_{Fe1}/\hat{V}_{Fe2}$ may be due to the increasing losses, which in the case of the dimensions 1 play a more important part because the volume 1 is larger. But the agreement with the equation derived on certain assumptions is poor.

3.2.4 Influence of the core material

The ferrite material is characterized by the magnetization curve B = f(H), which also includes the dependence $\mu_A = f(H)$. The static magnetization curves for the ferrites investigated are plotted in fig. 14-A. The decisive saturation inductions, which are characterized by the inequality $\frac{d\mu_A}{dH} < 0$ can be found from these curves.

The values were measured on demagnetized samples (new curves).

U 60	(μ_A = 9);	B_{sat} = 400 G
K 12	(μ_A = 24);	B_{sat} = 1000 G
K 1	(μ_A = 80);	B_{sat} = 2600 G
M 11	(μ_A = 250);	B_{sat} = 1800 G
M 33	(μ_A = 600);	B_{sat} = 2200 G
N 27	(μ_A = 2000);	B_{sat} = 2000 G
N 22	(μ_A = 2500);	B_{sat} = 2000 G
T 26	(μ_A = 2200);	B_{sat} = 1800 G
T 35	(μ_A = 5000);	B_{sat} = 2000 G

At high frequencies these values are lower. The difference between static and dynamic induction $\int B\,dB$ should be greater in the case of more permeable ferrites..

The saturation induction, which also governs the maximum peak voltage $\hat{V}_{Fe} \sim \sqrt{\int_{t=0}^{t=t_{sat}} B\,dB}$, is highest for the type K 1. With sufficient decoupling it is advisable to use this type. At the peak voltages ($\hat{V}_{Fe} \sim 50$ kV) necessary for start switches in the 40 kV region, the inductance of the ferrites (saturated) L_{Fe0} is about 10 ... 30 nHy.

./.

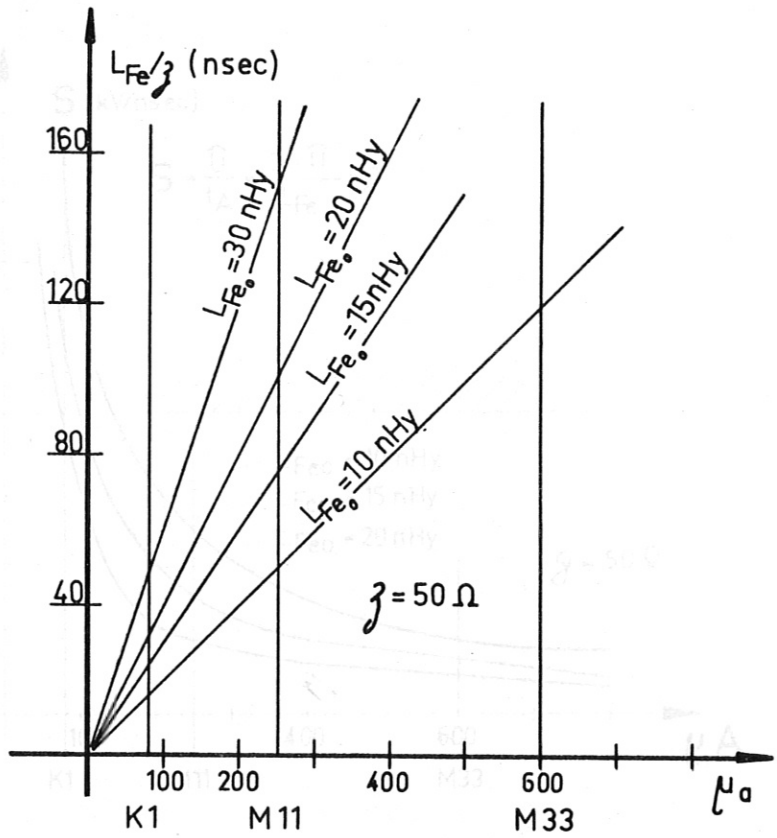

fig. 8: Decoupling time constant L_{Fe}/Z as a function of the core material and ferrite inductance (saturated) L_{Fe_o}

The resulting decoupling time constant L_{Fe}/Z are plotted in fig. 8 as functions of the material used and the inductance L_{Fe_o}.

For obvious reasons the pulse rise time t_A must be smaller than the decoupling time constant L_{Fe}/Z. If, for example, we set $t_A = 1/3 \cdot L_{Fe}/Z$ the minimum steepnesses calculated in fig. 9 as a function of the initial permeability are obtained.

It is found that at the inductances L_{Fe_o} = 10 ... 20 nHy that are expected the material K 1 does not decouple sufficiently.

In figs. 8-A and 9-A the maximum attainable voltages are plotted as functions of the ferrite material for various steepnesses. These functions have a pronounced maximum which shifts to less permeable values with increasing steepness. The peaks of these funktions $\hat{V}_{Fe} = f(\mu_A)$ are plotted in fig. 10 as functions of the pulse steepness S. With increasing pulse steepness this function

./.

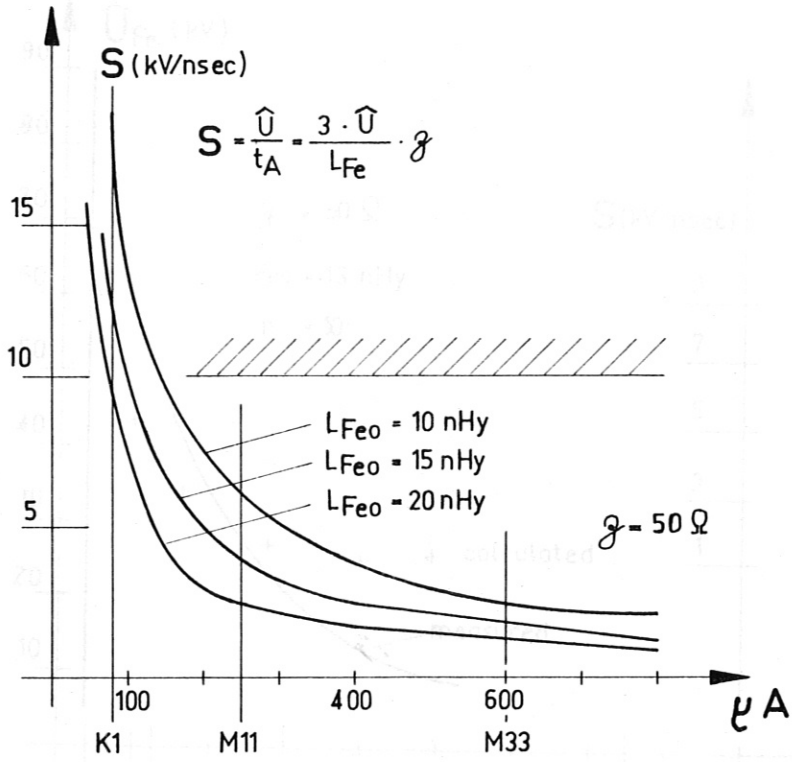

fig. 9: Required minimum pulse steepness as a function of the ferrite material

approaches core type K 1. The results evaluated here were measured on 10 ferrite cores (n = 10; L_{Feo} = 13 nHy). There is agreement with the function S = f(μ_A) calculated in fig. 9. The reasons already given for this characteristic behaviour appear to be correct.

It should also be mentioned that with increasing number of cores (n ↑ , L_{Feo} ↑) the decoupling necessarily assumes secondary significance. On the other hand, the losses and stray capacitances may exert a greater influence. Owing to the losses it may therefore be necessary to use low-loss cores (μ_A < 80), when a large number is required.

./.

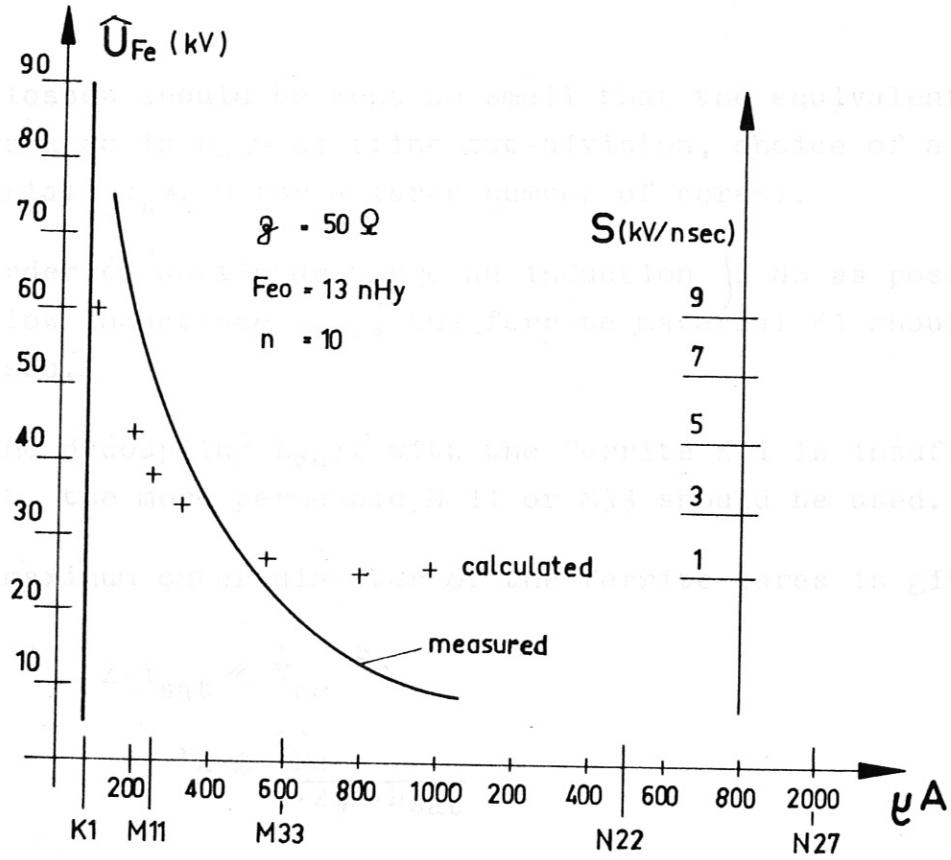

fig. 10: Optimum types of ferrite core as function of the steepness of the pulse

4. Dimensioning of a ferrite decoupling for spark gaps

1. The impedance of the trigger cable should be as low as possible (pulse sharpening, matching) $Z \triangleq 50\,\Omega$.

2. The trigger pulse should be as steep as possible. S = 5-10 kV/nsec (pulse sharpening).

3. The connection inductance L_A of the trigger cable should be kept low. ($L_A < 40$ nHy)

4. The stray capacitance of the ferrite arrangement should be kept so small that no resonance is possible with the trigger pulse

$$Z \cdot C_{Fe} \ll t_A$$

$$0{,}4 \cdot \pi \sqrt{L_A \cdot C_{Fe}} \ll t_A$$

./.

References

L 1: Roeder, Früngel:
Vortrag auf der Frühjahrstagung des Fachausschusses Plasmaphysik Bad Nauheim 1963

L 2: R. Wilhelm, H. Zwicker:
"Über eine einfache Kurzschluß-Funkenstrecke für Stoßstromanordnungen" - März 1965
Zeitschrift für angewandte Physik, 19. Band, 5. Heft

L 3: R.C. Kunze, E.v. Mark, H. Wedler, G. Klement:
"Ferrite Decoupled Crowbar Spark Gap"
Garching IPP 4/32 - April, 1966

L 4: R. Hancox:
"Switches for capacitor discharge duty;
III. High pressure switches"
Culham Laboratory - September, 1961

L 5: J. Gruber, G. Müller:
"Steep Voltage Triggering of a Simple Two-Electrode Crowbar Gap"
Garching IPP 4/27 - August, 1965

L 6: H. Häglsperger, G. Klement, R.C. Kunze, G. Müller:
"Combined Start and Crowbar Spark Gap with Wide Operating Range"
Garching IPP 4/28 - April, 1966

L 7: R.A. Fitch, N.R. McCormick:
"Low-Inductance Switching Using Parallel Spark Gaps"
The Institution of Electrical Engineers, Paper No. 3108
November, 1959

L 8: C. Petersen:
"Untersuchungen über die Zündverzugszeit von Dreielektrodenfunkenstrecken"
Dissertation, Techn. Hochschule Braunschweig
Oktober 1963

L 9: H. Zwicker, M. Kaufmann:
"Zum Mechanismus getriggerter Funkenstrecken"
Zeitschrift für Physik 180, 255-271
1964

gap problems	gap distance		spike formation
	electrode form		erosion
	electrode material		migration
	dielectric		
	insulation material		
	form of insulation		
pulse breakdown	irradiation	α, β, γ-photonen	static / pulsed
	field emission		
	pressure		
	pulse voltage steepness		
	dielectric (air, SF6, frigen, ...)		
	gap distance		
decoupling arrangement	ferrite material		
	ferrite dimensions		
	number of ferrites		
trigger system	pulse voltage steepness		
	impedance of trigger cable		
	premagnetization, pulse sharpening, matching		

fig. 1-A: Variable parameters of an overvolted two-electrode spark gap with saturable inductance

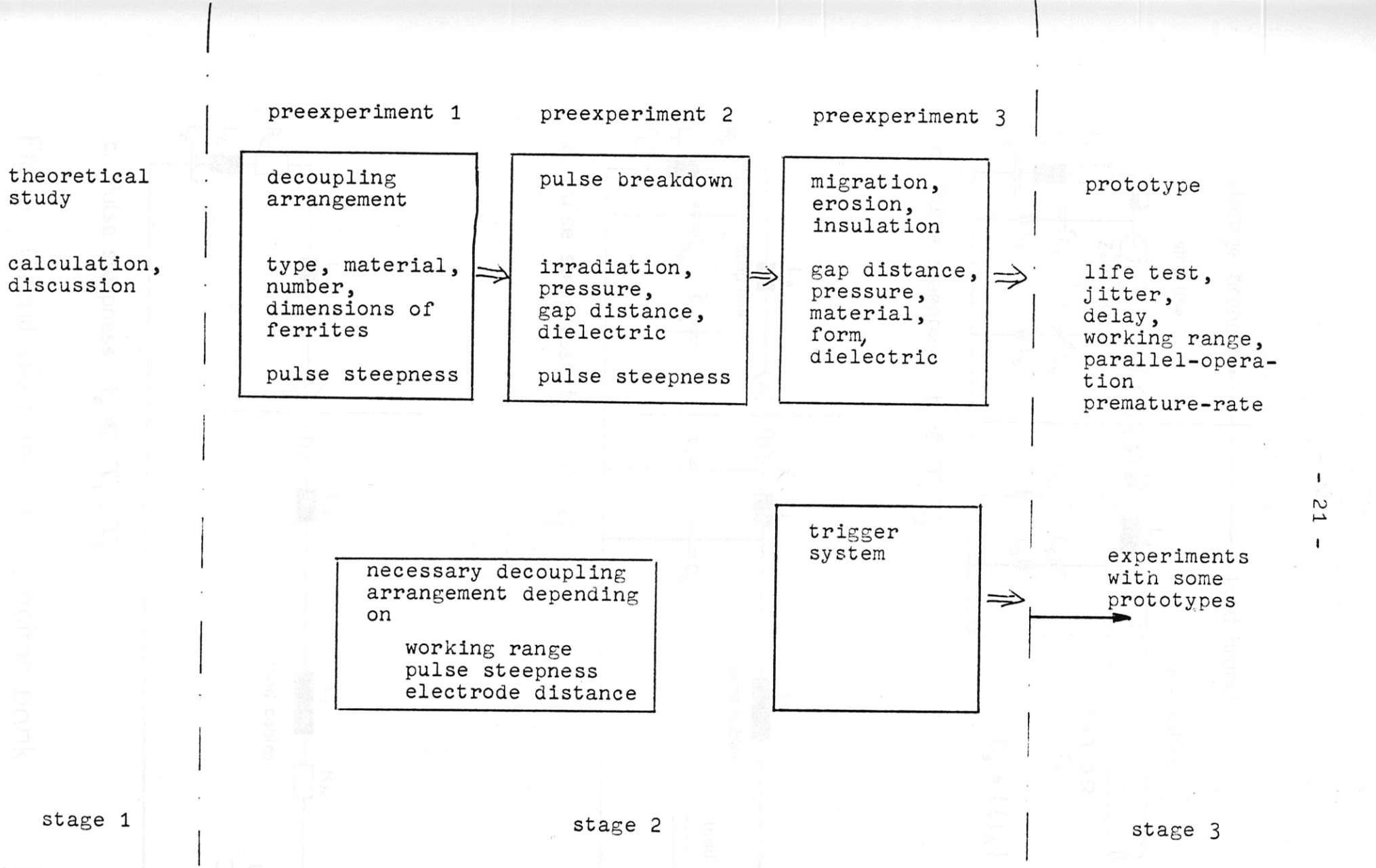

fig. 2-A: Schematic diagram with different development stages of a pressurized, overvolted, two-electrode spark gap for heavy duty.

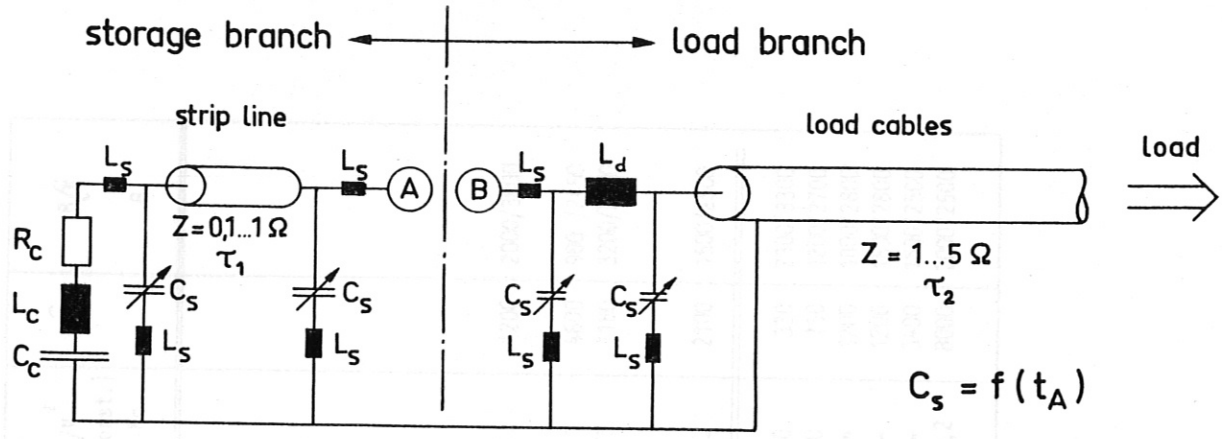

a. Pulse steepness $t_A \ll \tau_1, \tau_2$

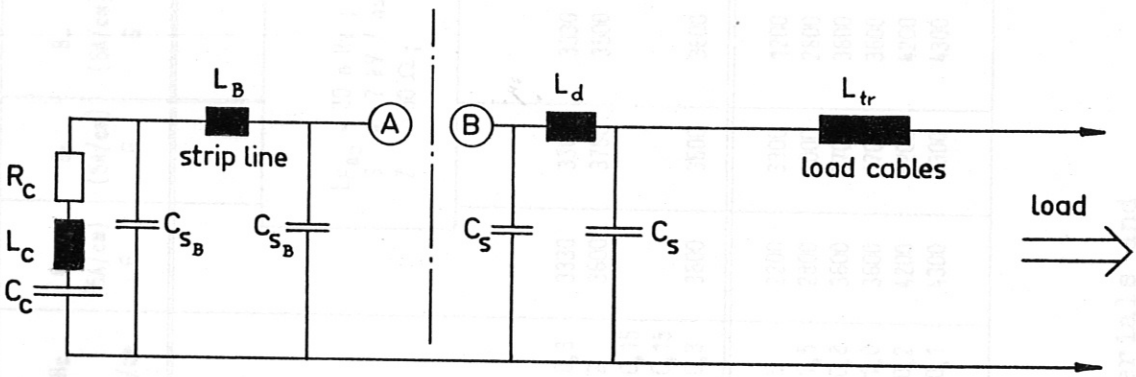

b. Pulse steepness $t_A \sim \tau_1, \tau_2$

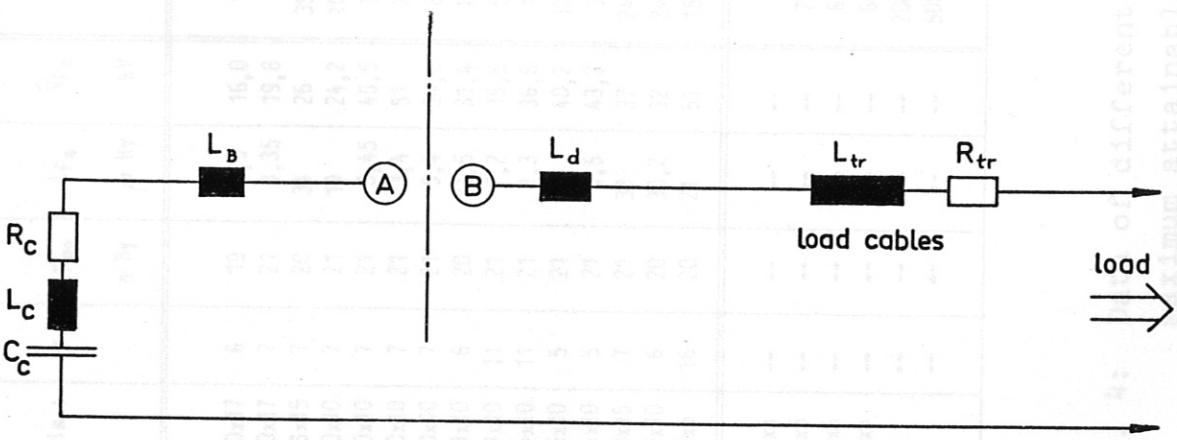

c. Pulse steepness $t_A \ll \tau_1, \tau_2$

Fig. 3 Circuit diagram of capacitor bank

Type	Dim.:	n	L_{Fe_o} n Hy	L_{Fe} μ Hy	$\hat{V}_{Fe}$ kV	μ_A	fmax Mc	Hc A/cm	B_o (5A/cm) G	B_+ (5A/cm) G	B_- (5A/cm) G	B (10A/cm) G	μ' (const.) Mc	$\hat{\mu}$	$B\hat{\mu}$ G
Gecalloy G 10S	51x30x17	6	19	0,5	16,0	145									
Gecalloy G 10Y	51x30x17	7	21	1,35	19,8	89									
Valvo A 4A	36x23x15	7	20	34	26	3558									
Mitsubishi LM	51x20x10	7	21	19	24,2	1000									
Mitsubishi LS	51x20x10	7	21	3,45	45,5	500									
Mitsubishi LC	49x20x10	7	21	3,4	51	200									
Mitsubishi LNB	50x20x10	7	21	5,4	34,6	800									
Mitsubishi LN	70x23x10	6	20	21,5	31,4	800									
Stemag 610	36x23x10	11	21	7,2	35,5	550								1200	2000/3000
Stemag	38x24x10	11	21	1,3	36,6	125									
Krupp E 2	50x15x10	5	21	18	40,2	1000	0,5	0,3	3330	3360	3330		1	4600	900 /2450
Krupp E 4	52x15x10	5	21	3,5	43,2	300	2,5	2	3600	3750	3500		5	1180	3200/3500
Krupp D 1S2	79x40x15	7	21	38	37	2400		0,15							
Krupp D 1S2	51x18x10	6	20	30,2	32	2400		0,15							
Siemens N 22	72x30x5	16	20	21	51	1500	0,2	0,3	3600	3600	3600		2	2100	1500/2500
Siemens K 1	72x30x5	--	--	--	--	80	0,12	5	2200	3300	1200		40	330	2300/3300
Siemens M 11	72x30x5	--	--	--	--	250	2	1,5	2800	3000	2800		10	750	1200/2700
Siemens M 25	72x30x5	--	--	--	--	650	1,6	0,8	3600	3700	3600		4	1200	1800/2800
Siemens M 33	72x30x5	--	--	--	--	600	1,0	1,0	3600	3700	3600		--	1200	1800/2800
Siemens N 27		--	--	--	--	2000		0,2	4200	4200	4200		--	3400	1500/2500
Siemens T 35		--	--	--	--	5000		0,1	4300	4300	4300		0,2	8000	2000/2500

L_{Fe_o} = 20 n Hy ;
S = 7 kV / nsec
Z = 50 Ω ;

fig. 4: Data of different ferrite-materials and maximum attainable voltage $\hat{V}_{Fe}$ (kV).

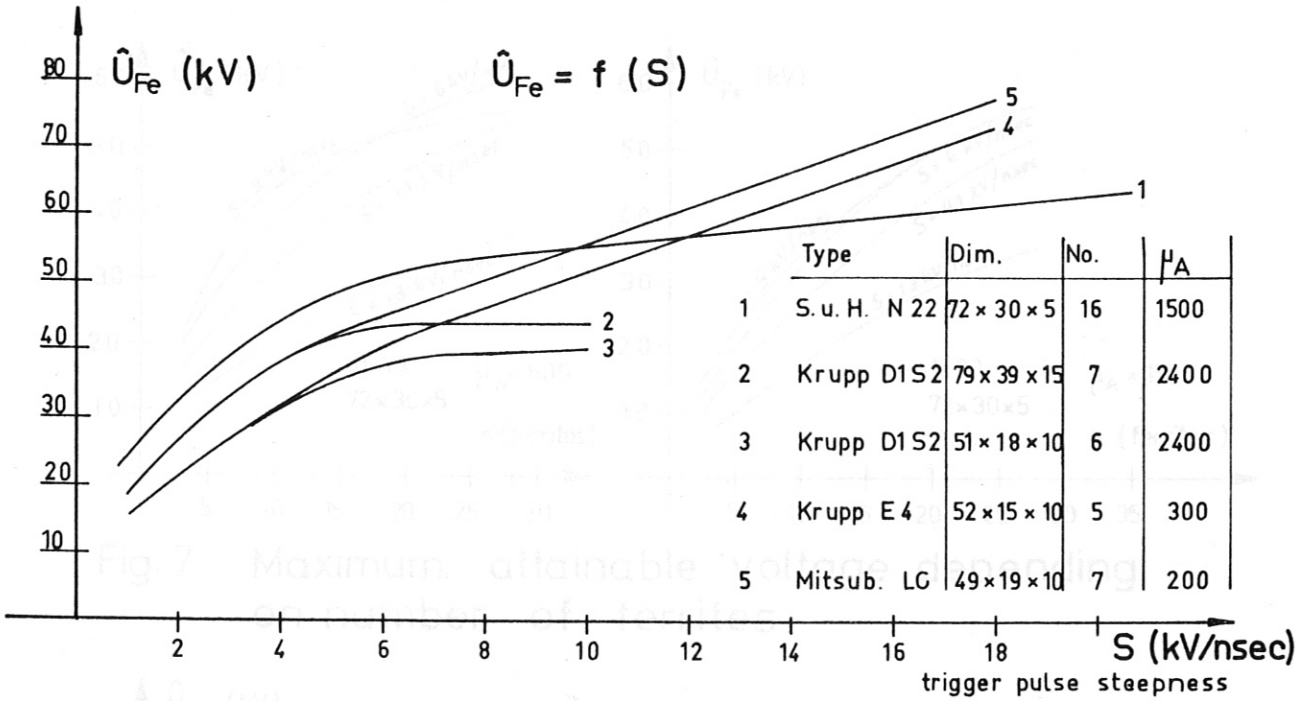

	Type	Dim.	No.	μ_A
1	S.u.H. N 22	72 × 30 × 5	16	1500
2	Krupp D1S2	79 × 39 × 15	7	2400
3	Krupp D1S2	51 × 18 × 10	6	2400
4	Krupp E4	52 × 15 × 10	5	300
5	Mitsub. LG	49 × 19 × 10	7	200

Fig. 5 Maximum attainable voltage $\hat{U}_{Fe}$ depending on pulse steepness

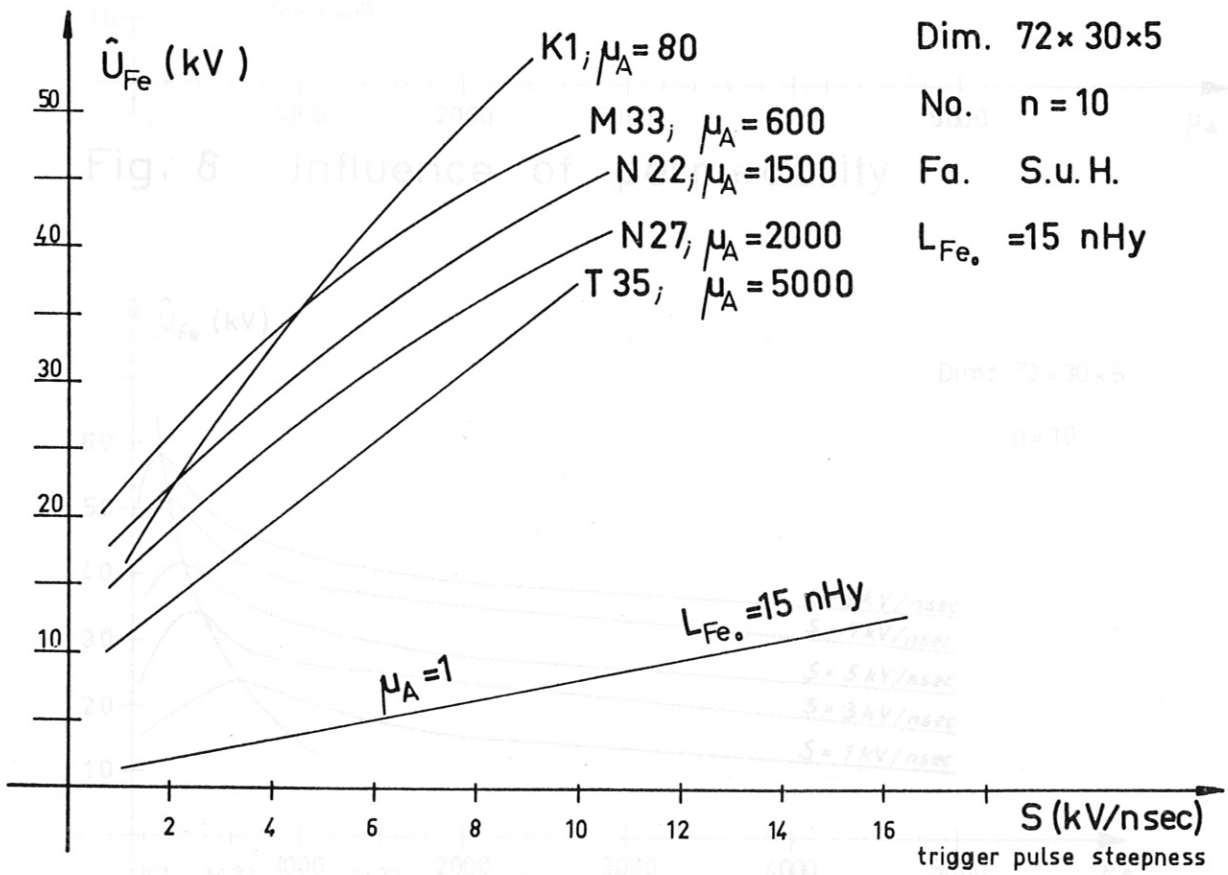

Fig. 6 Jnfluence of ferrite material

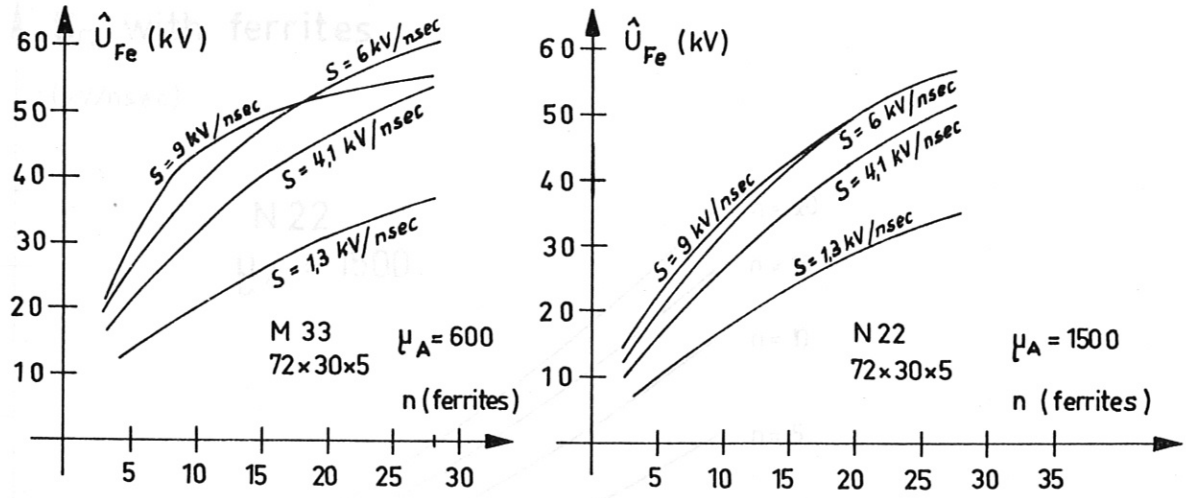

Fig. 7 Maximum attainable voltage depending on number of ferrites

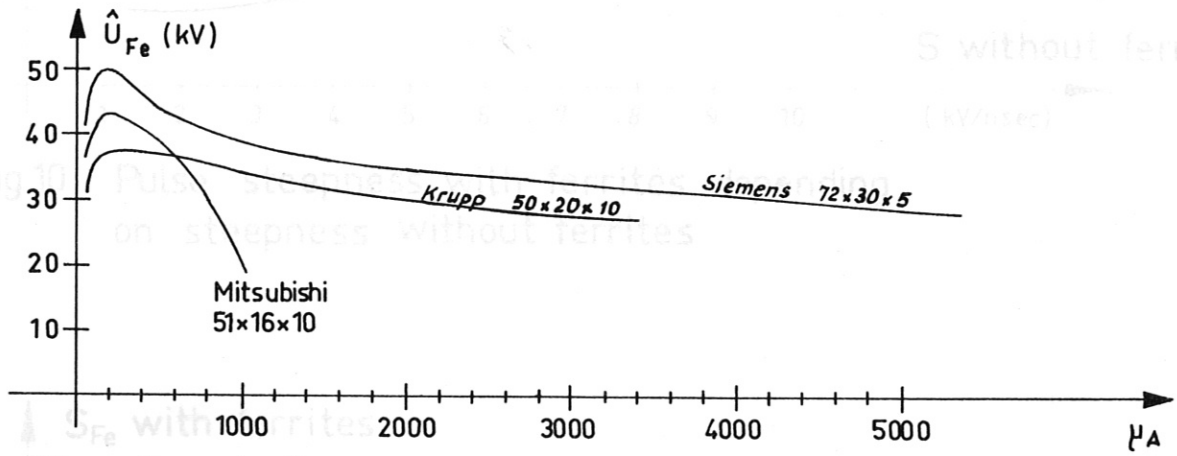

Fig. 8 Jnfluence of permeability

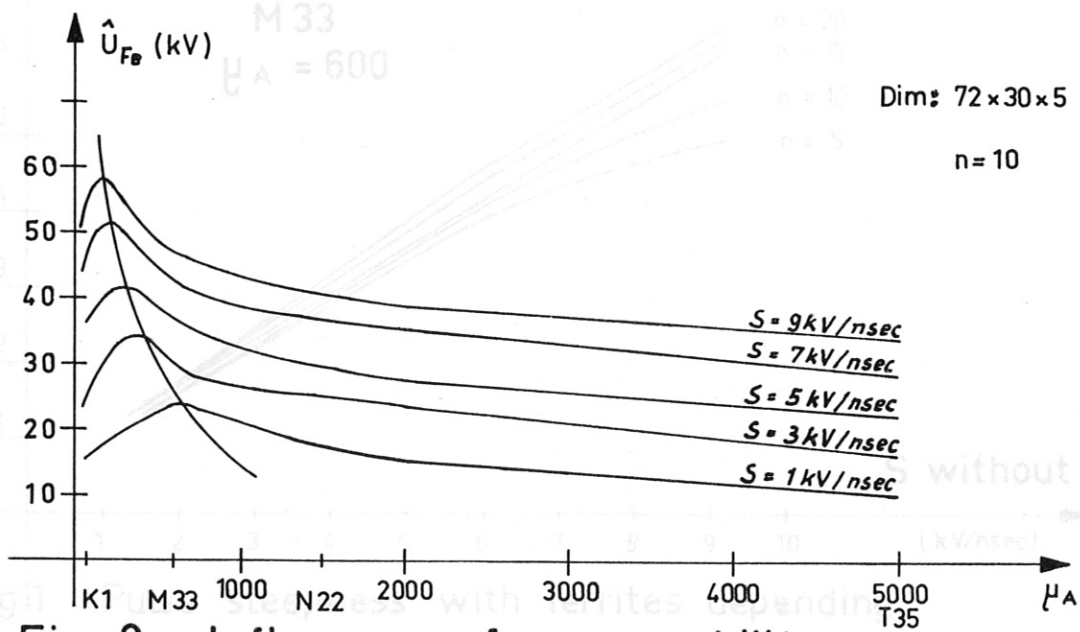

Fig. 9 Jnfluence of permeability

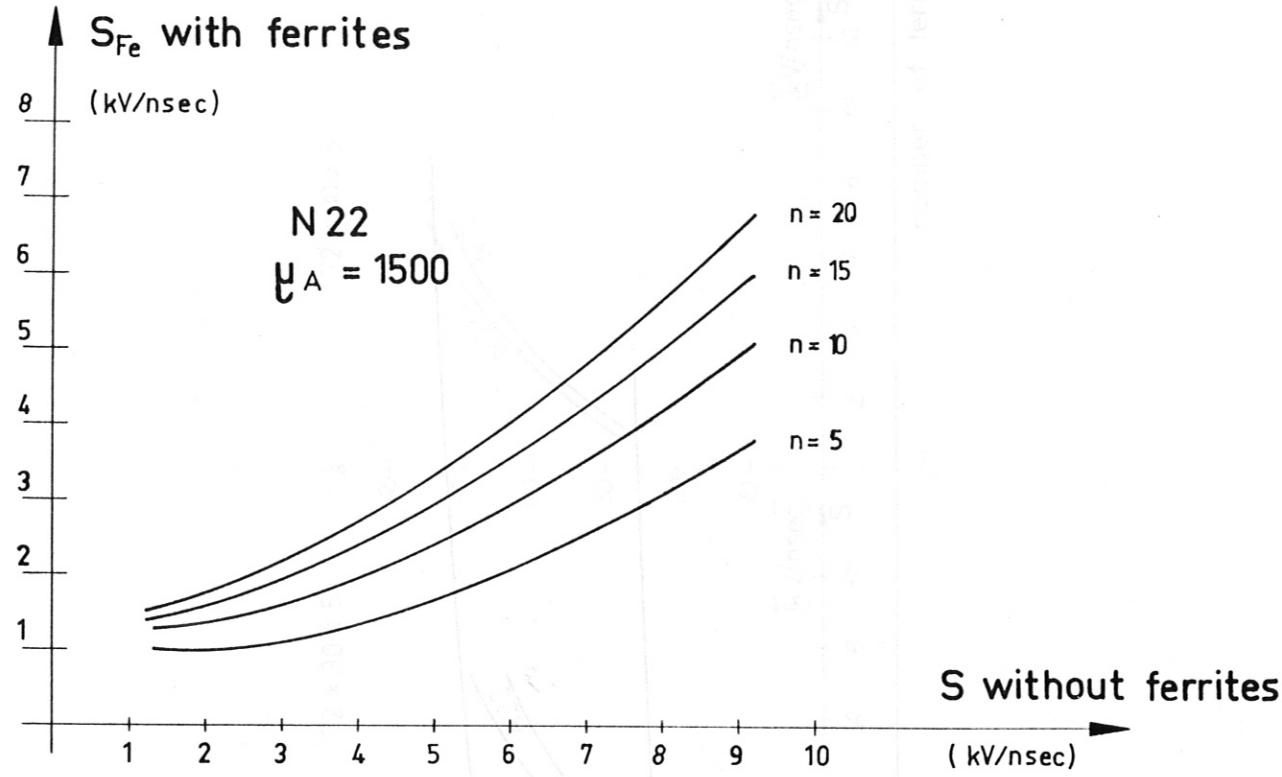

Fig 10 Pulse steepness with ferrites depending on steepness without ferrites

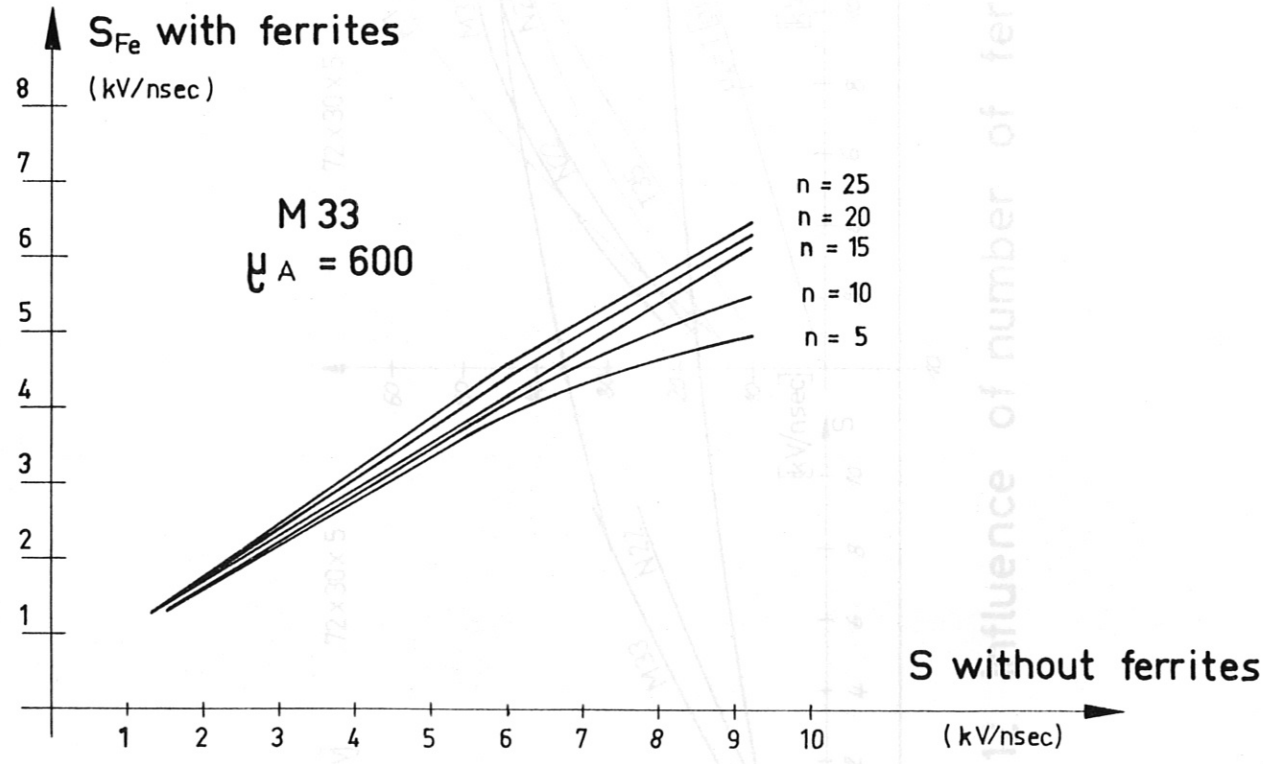

Fig11 Pulse steepness with ferrites depending on steepness without ferrites

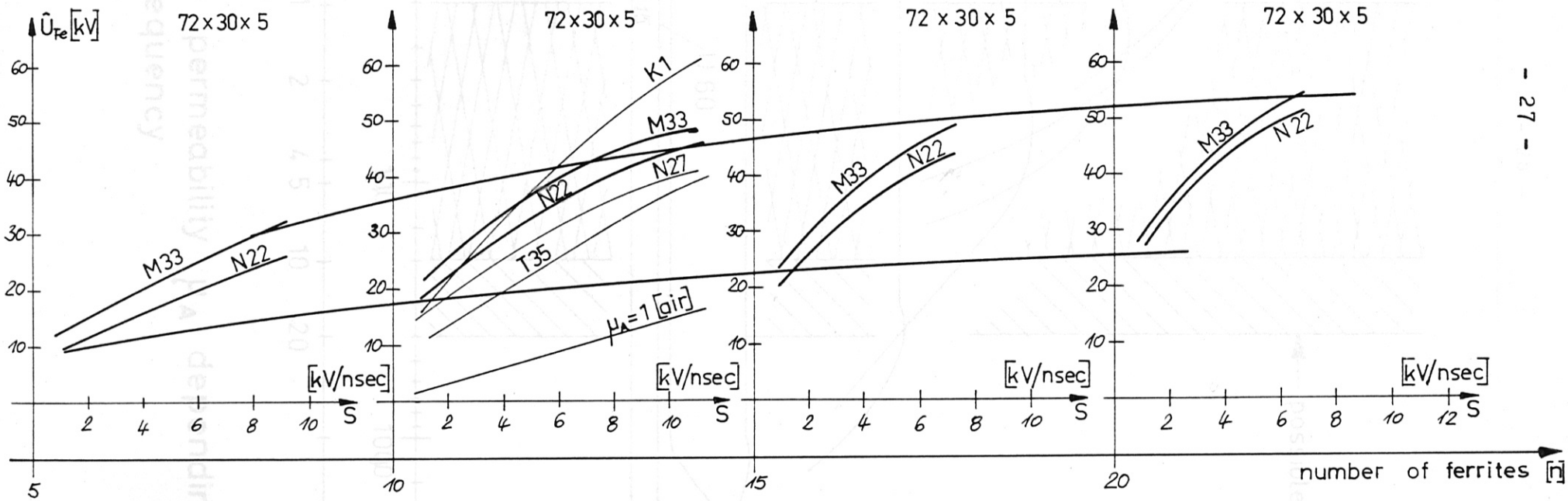

Fig: 12 Influence of number of ferrites

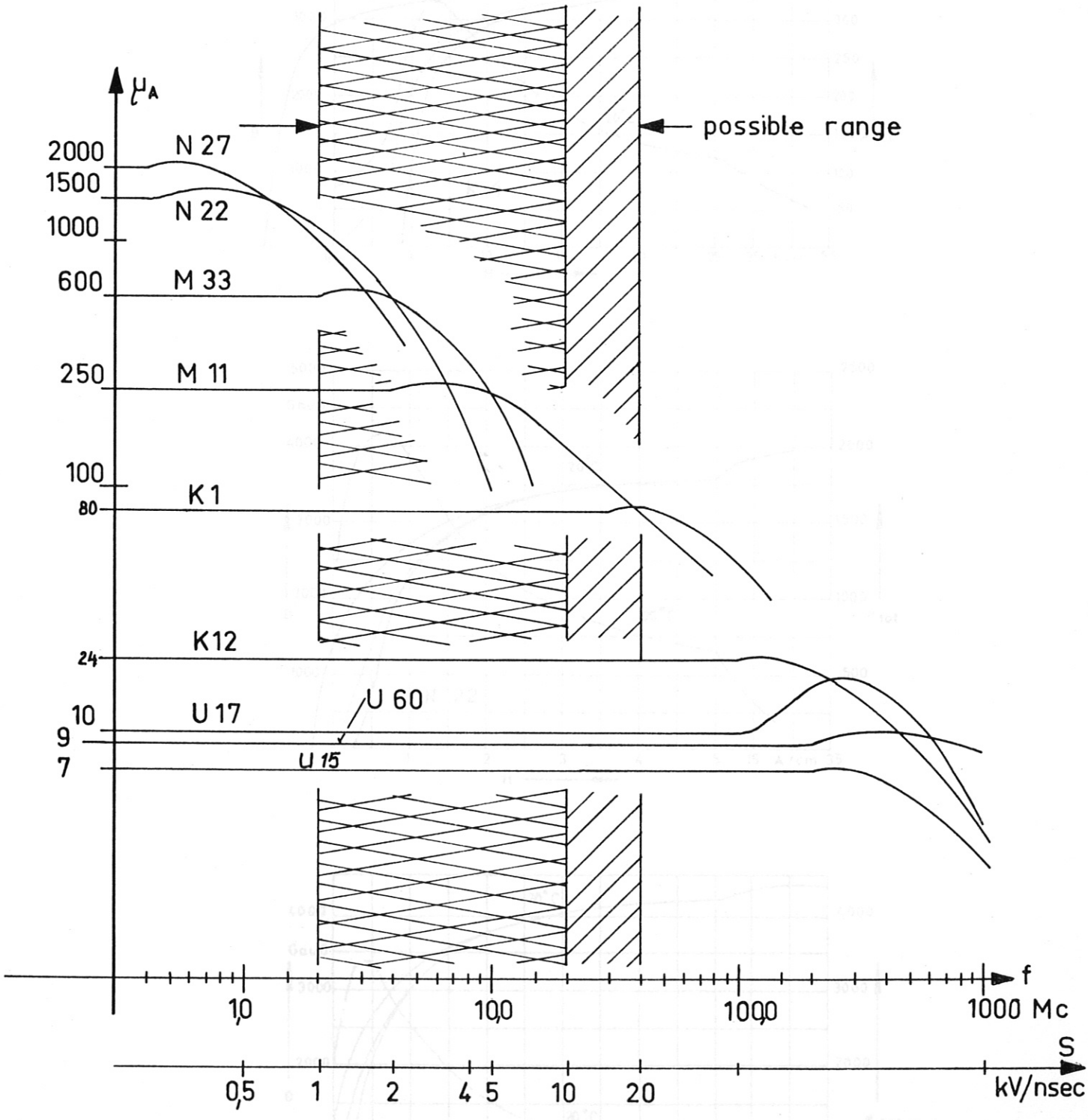

Fig. 13 Ferrite permeability μ_A depending on frequency

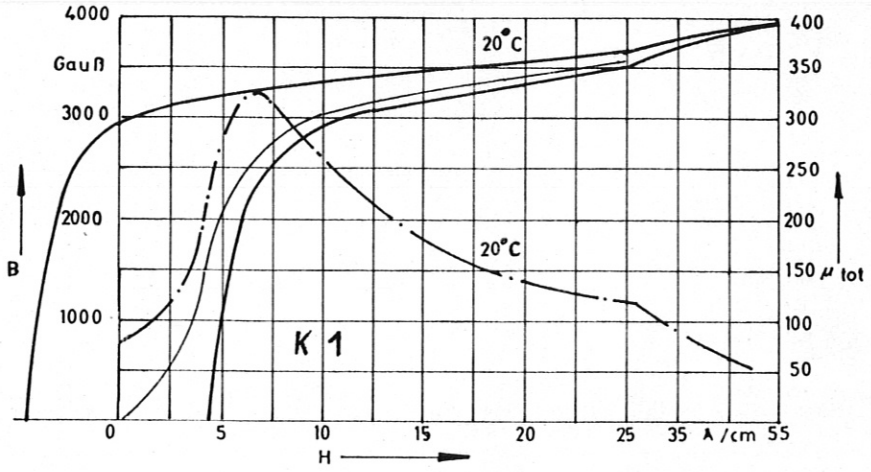

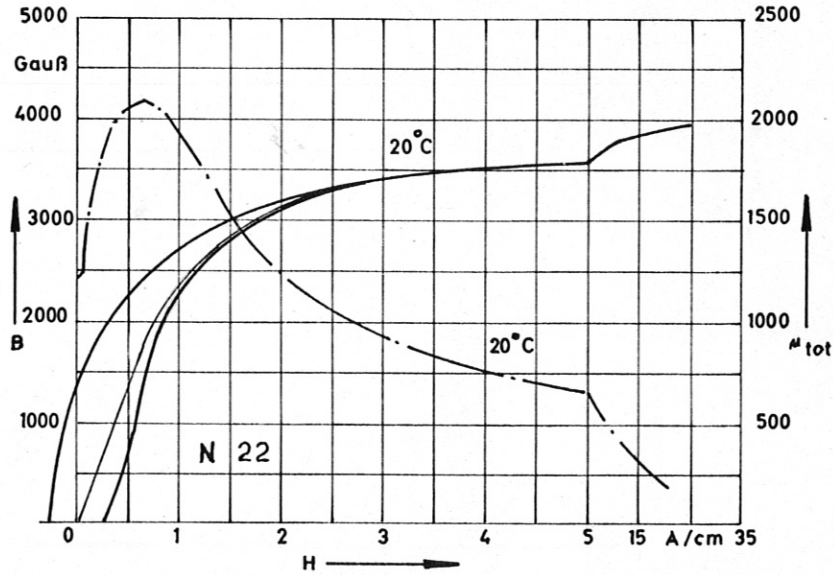

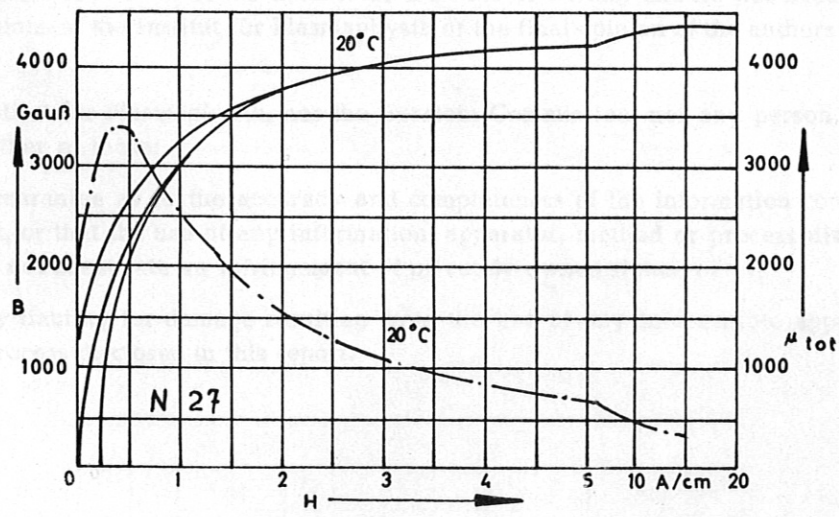

fig. 14: Static B-H curves for various ferrite-materials